J. Fluid Mech. (1984), *vol.* 140, *pp.* 113–133
Printed in Great Britain

Influence of non-uniform temperature distribution on the steady motion of ice sheets

By L. W. MORLAND AND G. D. SMITH
School of Mathematics and Physics, University of East Anglia, Norwich NR4 7TJ, U.K.

(Received 22 July 1983)

The plane steady flow of a grounded ice sheet is analysed under the assumption that the ice behaves as a nonlinearly viscous fluid with a strongly temperature-dependent rate factor. It is supposed that the accumulation/ablation distribution on the (unknown) free surface is prescribed, and that there is a given basal sliding condition connecting the tangential velocity, tangential traction and normal pressure. The basal boundary is defined as the smooth contour which describes the mean topography viewed on the ice-sheet lengthscale, and is assumed to have small slope. The perturbation analysis which reduces the isothermal or constant rate factor equations to an ordinary differential equation for the leading-order profile is now extended with similar success to the non-isothermal problem when the temperature distribution is prescribed. That is, the thermomechanically coupled energy balance is not solved, but families of temperature distributions qualitatively compatible with observed patterns are adopted to exhibit the effects of significant creep-rate variation with temperature.

1. Introduction

Large ice sheets have significant temperature variation with depth, with melting or near-melting temperatures in some basal regions to 30 K or more colder temperatures at the surface, but more modest temperature gradients over their much greater spans. Heat advection is a dominant contribution to the overall energy balance, and the viscous shear response of ice is strongly temperature dependent, so a solution of the full thermomechanically coupled energy and momentum equations is required to determine a valid temperature field. However, observation has indicated qualitative features of temperature distributions, and here we adopt a series of temperature patterns to investigate the influence of temperature on profiles and flows determined by the mass and momentum balances.

The temperature-dependent rate factor describes a decreasing viscosity as temperature increases, with the most rapid rate of decrease occurring as melting is approached. It is therefore clear that the most significant temperature effect will arise in near-temperate zones, which would be located in basal regions. This suggests that the higher shear-strain rates would occur in the warmer basal regions, and that the differential motion between the surface and an upper boundary of this basal shear layer would be relatively small. Nye's (1959) pioneering model of ice-sheet flow adopts the extreme approximation that there is no differential motion between surface and base; that is, the longitudinal velocity is independent of depth. The shear flow is relegated to a *thin* warm basal layer, and its effect is described only through a basal sliding law. The consequence of this extreme approximation is that the internal flow is independent of the viscous response of the ice. Here we are able to demonstrate

that the profile and flow for a given accumulation/ablation distribution and given sliding law depend significantly on the temperature distribution, and that the basal layer of high strain-rate gradient which can occur is not generally thin enough to be modelled by such a discontinuity. It must be concluded that an elementary model that neglects the shearing throughout the ice sheet cannot, in general, provide a satisfactory description of either flow or profile.

Plane steady flow of an isothermal sheet or for temperature-independent ice creep has been successfully treated by a perturbation analysis (Morland & Johnson 1980, 1982), which yields a second-order ordinary differential equation, subject to determined initial conditions at a margin, for the leading-order profile function. That is, the system of elliptic partial differential equations on an unknown domain is reduced to a standard initial-value problem for an ordinary differential equation. The small parameter, which is determined by magnitudes of material parameters and prescribed boundary conditions, is a measure of the small surface-slope magnitude. Such neglect of temperature effects is unrealistic except for a near-temperate glacier, but the same variable and coordinate scalings implied by the mass and momentum balances follow also for a general unsteady, thermomechanically coupled flow problem (Morland 1983), and the leading-order steady plane flow is described by a simpler, parabolic system of partial differential equations.

Hutter (1982) proposed that the thermomechanical problem for a steeply inclined bed, which has simpler expressions for the stress and velocity in terms of the unknown profile, can be treated as a sequence of mechanical problems with prescribed temperature field and prescribed surface profile, and outlines an approach in his recent (1983) text. The temperature field and profile at each stage are to be recalculated using the previous stress and velocity fields, but the initial approximate solution involves the assumption of both temperature field and surface profile. Here we uncouple the energy and momentum equations by prescribing a temperature field, but show that the mechanical problem for the leading-order stress and velocity fields and unknown profile again reduces to a second-order differential equation subject to two boundary conditions at one margin. Solutions for different assumed temperature patterns are determined to display the influence of temperature distribution on velocity fields and profile. While the energy balance could now be used to construct an iteration scheme for the temperature field to treat the thermomechanically coupled flow, direct numerical solution of the parabolic system (Morland 1983) appears to be a more attractive proposition.

The temperature patterns used for the illustrations have the following features:

(i) The surface temperature decreases with height at a rate 0.8 K per 100 m, and the vertical temperature gradient at the surface is zero, reflecting negligible heat conduction from the surface.

(ii) Alternative values of -1 K per 100 m and -2.5 K per 100 m are assumed for the vertical temperature gradient at the base, reflecting respective geothermal heat fluxes of 0.8×10^6 J m^{-2} a^{-1} and 2.0×10^6 J m^{-2} a^{-1} if frictional heating and dissipation are negligible at the base.

(iii) Four patterns of basal temperature distribution are considered:

(*a*) uniform;

(*b*) monotonic decreasing from the margin;

(*c*) monotonic increasing from the margin;

(*d*) monotonic increasing from the margin followed by a monotonic decreasing stage.

Results and comparisons show distinct profile and flow solutions from the different patterns.

The first sliding law used is that inferred by Morland, Smith & Boulton (1983) from data for the 70° N section of the Greenland Ice Sheet, but based on the isothermal (mean-temperature) analysis of Morland & Johnson (1980, 1982). We next prescribe a temperature distribution for the Greenland Ice Sheet section, and use the present temperature-dependent analysis with the profile and accumulation data to determine a modified sliding law. Repeating some of the above illustrations with the modified law shows little difference in the overall results, and we deduce that details of the sliding law when sliding velocities are relatively small away from the margins, have little large-scale influence. Away from the margin, a simple no-slip condition may be the most satisfactory approximation for the basal boundary condition.

2. Ice properties

We make the conventional assumption that, on the long timescales of material ice flows, the ice responds as an incompressible nonlinearly viscous fluid with a temperature-dependent rate factor and with deviatoric stress and strain rate parallel. The deviatoric stress $\boldsymbol{S}$ and mean pressure p are related to the stress $\boldsymbol{\sigma}$ by

$$\boldsymbol{S} = \boldsymbol{\sigma} + p\boldsymbol{I}, \quad p = -\tfrac{1}{3}\operatorname{tr}\boldsymbol{\sigma}, \quad \operatorname{tr}\boldsymbol{S} = 0. \tag{1}$$

Let $\boldsymbol{D}$ be the strain rate, given by the spatial gradient of the velocity field $\boldsymbol{v}$, and let T denote temperature. The viscous shear response is described by the equivalent relations

$$\frac{\boldsymbol{D}}{D_0} = a(T)\,\omega(J)\frac{\boldsymbol{S}}{\sigma_0}; \quad \frac{\boldsymbol{S}}{\sigma_0} = \frac{\phi(\hat{I})}{a(T)}\frac{\boldsymbol{D}}{D_0}, \tag{2}$$

where

$$J = \tfrac{1}{2}\operatorname{tr}\left(\frac{\boldsymbol{S}}{\sigma_0}\right)^2, \quad \hat{I} = \tfrac{1}{2}\operatorname{tr}\left(\frac{\boldsymbol{D}}{D_0\,a(T)}\right)^2, \tag{3}$$

and σ_0 and D_0 are respectively stress and strain-rate units chosen to normalize the relations (2). While, in general, there is no explicit inversion between the material functions $\phi(\hat{I})$ and $\omega(J)$, there are important implicit reciprocal relations which follow from the equivalent relations (2), namely

$$\phi(\hat{I})\,\omega(J) = 1, \tag{4}$$

$$\hat{I} = J\omega^2(J) = G(J), \quad J = \hat{I}\phi^2(\hat{I}) = G^{-1}(\hat{I}). \tag{5}$$

With the units

$$\sigma_0 = 10^5\ \mathrm{N\ m^{-2}}, \quad D_0 = 1\ \mathrm{a^{-1}} = 3.18\times10^{-8}\ \mathrm{s^{-1}}, \tag{6}$$

Glenn's (1955) uniaxial compression data at 273.13 K has an excellent polynomial approximation (Smith & Morland 1981)

$$\omega(J) = 0.3336 + 0.3200J + 0.02963J^2, \tag{7}$$

over the shear-stress range 0–5×10^5 N m^{-2}, particularly at the low shear stresses typical in natural ice flows. For shear-stress magnitudes below $2\sigma_0$ ($J \leqslant 4$) we see that both $\omega(J)$ and its derivative $\omega'(J)$ are order unity, but also that $\phi(0) = 1/\omega(0)$ is of order unity (and non-zero), which reflects a bounded viscosity at zero stress. A conventional power-law representation with exponent greater than unity implies unbounded $\phi(0)$, and in turn unbounded longitudinal stress at the free surface in the leading-order isothermal solution (Morland & Johnson 1982), which can be removed only by a surface boundary layer of high stress gradient (Johnson & McMeeking 1982). Such singular behaviour is not physically expected, and the associated singular perturbation analysis and asymptotic matching adds considerable complexity to even

$\bar{T}$	$\bar{a}$	$\bar{a}'$	$\bar{a}'/a$
0	1.068	9.673	9.057
−0.5	0.0805	0.254	3.155
−1.0	0.0180	0.053	2.949
−1.5	0.00412	0.0122	2.949
−2.0	0.00094	0.00277	2.949

TABLE 1. The rate factor $\bar{a}(\bar{T})$ and its gradient

the steady isothermal flow solution. On both counts the polynomial representation (7) is more satisfactory, in addition to providing the better data correlation.

Mellor & Testa's (1969) uniaxial compression data at constant stress and constant temperatures over the wide range 212–273 K have been closely correlated by a rate factor (Smith & Morland 1981)

$$\left.\begin{aligned} a(T) &= a_0\,\bar{a}(\bar{T}), \quad T = 273.15\,\mathrm{K} + (20\,\mathrm{K})\,\bar{T}, \\ \bar{a}(\bar{T}) &= 0.7242\,\mathrm{e}^{11.9567\bar{T}} + 0.3438\,\mathrm{e}^{2.9494\bar{T}}. \end{aligned}\right\} \tag{8}$$

Here $a(273\ \mathrm{K}) = a_0$, while the laboratory data was normalized on $a(273\ \mathrm{K}) = 1$. The additional scale factor $a_0\ (\leqslant 1)$ is introduced to achieve the lower strain rates at given stress inferred from ice-shelf data in comparison with Glen's laboratory data. An equivalent device was adopted by Morland *et al.* (1983) in an estimation of basal sliding velocities from the ice-sheet data, where the assumed isothermal temperature of the Greenland Ice Sheet was reduced to ensure sliding in the sensible direction everywhere. We regard a reduction factor $a_0 = 0.2$ as a lower limit for consistency with ice-shelf data (Morland & Shoemaker 1982). The values of $\bar{a}(\bar{T})$ and its gradient over the temperature range 233.15–273.15 K are illustrated in table 1. The most rapid decrease occurs near melting ($\bar{T} = 0$), but the relative gradient $\bar{a}'/\bar{a}$ which influences the relative strain-rate gradient only reaches a value 9 at melting and has a nearly uniform value 3 below 263 K.

3. Balance equations and boundary conditions

We will consider the steady configuration of an ice sheet with flow confined to the plane Oxy of rectangular coordinates $Oxyz$, where Oy is vertically upwards. The fixed basal boundary is given by $y = f(x)$, which is a smooth contour of (assumed) small slope reflecting the mean topography on the sheet lengthscale. The profile surface $y = h(x)$ is traction-free, and must be determined by the kinematic condition describing the accumulation/ablation distribution. We introduce dimensionless coordinates with respect to a thickness magnitude d_0, dimensionless velocities with respect to an accumulation magnitude q_m, and dimensionless stress with respect to an overburden pressure magnitude $\rho g d_0$, where g is the constant acceleration due to gravity and ρ is the (assumed) constant ice density 918 kg m^{-3}. Thus

$$\left.\begin{aligned} (x, y) &= d(\bar{x}, \bar{y}), \quad f(x) = d_0 \bar{f}(\bar{x}), h(x) = d_0 \bar{h}(\bar{x}), \\ (u, v) &= q_\mathrm{m}(\bar{u}, \bar{v}), \quad (q, b) = q_\mathrm{m}(\bar{q}, \bar{b}), \\ (\boldsymbol{\sigma}, p, \boldsymbol{S}) &= \rho g d_0 (\bar{\boldsymbol{\sigma}}, \bar{p}, \bar{\boldsymbol{S}}), \quad \boldsymbol{D} = \frac{q_\mathrm{m}}{d_0}\bar{\boldsymbol{D}}, \end{aligned}\right\} \tag{9}$$

where (u, v) are the in-plane velocity components, q is the accumulation density (volume flux of ice entering the sheet in unit time per unit horizontal cross-section), b is the basal drainage density (volume flux of ice leaving the sheet in unit time per unit horizontal cross-section), and q_m/d_0 is the strain-rate unit for $\bar{\boldsymbol{D}}$.

Mass balance, or incompressibility, is given by

$$\operatorname{tr}\bar{\boldsymbol{D}} = \frac{\partial \bar{u}}{\partial \bar{x}} + \frac{\partial \bar{v}}{\partial \bar{y}} = 0, \tag{10}$$

which is satisfied by a stream-function representation

$$\bar{u} = \frac{\partial \bar{\psi}}{\partial \bar{y}}, \quad \bar{v} = -\frac{\partial \bar{\psi}}{\partial \bar{x}}. \tag{11}$$

The momentum balance for the very slow viscous flow of a natural ice mass under gravity reduces to the equilibrium equations

$$\frac{\partial \bar{\sigma}_{xx}}{\partial \bar{x}} + \frac{\partial \bar{\sigma}_{xy}}{\partial \bar{y}} = 0, \quad \frac{\partial \bar{\sigma}_{xy}}{\partial \bar{x}} + \frac{\partial \bar{\sigma}_{yy}}{\partial \bar{y}} = 1. \tag{12}$$

Let (n, s) denote a right-handed local coordinate system with n pointing normally out from the sheet on both surface and base. The concepts of sliding velocity and a sliding law on a smoothed basal boundary for the ice-sheet domain, which ignores details of small-scale topography, have been discussed in detail by Morland *et al.* (1983), and are adopted here. If $\beta = \bar{f}'(\bar{x})$ is the bed slope, then the basal drainage condition is

$$\beta \bar{u} - \bar{v} = \bar{b} \quad (\bar{y} = \bar{f}), \tag{13}$$

while the tangential (sliding) velocity $\bar{u}_s$ is given by

$$-(1+\beta^2)^{\frac{1}{2}}\,\bar{u}_s = \bar{u} + \beta \bar{v} \quad (\bar{y} = \bar{f}). \tag{14}$$

The normal and tangential tractions on the ice at the bed, $\bar{t}_n$, $\bar{t}_s$, are given by

$$\left.\begin{aligned} (1+\beta^2)\,\bar{t}_n &= \beta^2 \bar{\sigma}_{xx} + \bar{\sigma}_{yy} - 2\beta \bar{\sigma}_{xy}, \\ (1+\beta^2)\,\bar{t}_s &= \beta(\bar{\sigma}_{yy} - \bar{\sigma}_{xx}) + (1-\beta^2)\,\bar{\sigma}_{xy} \end{aligned}\right\} \quad (\bar{y} = \bar{f}). \tag{15}$$

The tangential traction $-\bar{t}_s$ of the ice on the bed, has the same direction as the tangential velocity $\bar{u}_s$, and we adopt a sliding law with the separable form

$$\bar{t}_s = \bar{t}_n\, \mu(-\bar{t}_n)\, \bar{u}_s \quad (\bar{y} = \bar{f}), \tag{16}$$

where $-\bar{t}_n$ is the positive basal pressure and $\mu(0)$ is bounded. The limit behaviour $\bar{t}_s \to 0$ linearly with $\bar{t}_n$ is compatible with a small surface-slope profile up to the margin (Morland & Johnson 1980, 1982). Linearity between $\bar{t}_s$ and $\bar{u}_s$ is not essential, but has provided the most satisfactory correlation with Greenland and Devon Ice Cap data (Morland *et al.* 1983) using the isothermal theory. We adopt the form deduced from the Greenland data for our illustrations, noting that large variations of the function $\mu(-\bar{t}_n)$ result only in modest changes of the isothermal solution (Boulton, Smith & Morland 1983). Thus

$$\mu(k^{-1}\tilde{p}_b) = 2.5 \times 10^{-5}\, \tilde{\mu}(\tilde{p}_b), \quad k = \frac{\rho g d_0}{2 \times 10^7\ \mathrm{N\,m^{-2}}} = O(1), \tag{17}$$

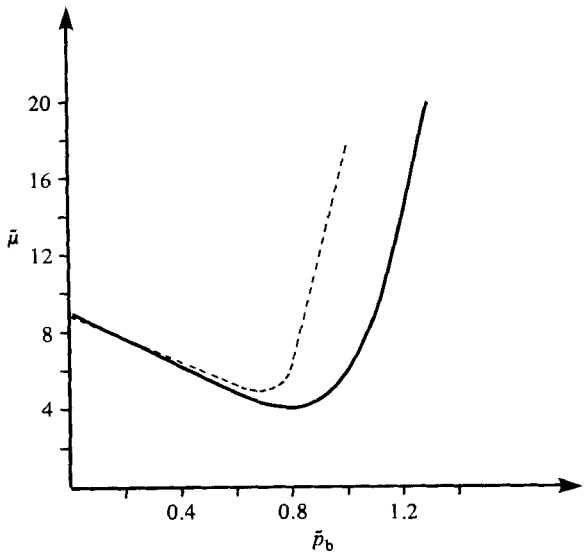

FIGURE 1. The sliding function $\tilde{\mu}(\tilde{p}_b)$: ——, isothermal deduction; - - - - -, thermal deduction.

$$\left.\begin{aligned}\tilde{\mu}(\tilde{p}_b) &= 9.0-6.657\tilde{p}_b \quad (0 \leqslant \tilde{p}_b \leqslant 0.7),\\ &= \sum_{t=0}^{5} \mu_t \tilde{p}_b^t \quad (0.7 \leqslant \tilde{p}_b \leqslant 1.3),\\ &= 19.73+54.43(\tilde{p}_b-1.3) \quad (\tilde{p}_b \geqslant 1.3),\\ \mu_0 &= -53.596, \quad \mu_1 = 253.643, \quad \mu_2 = -324.134,\\ \mu_3 &= 26.753, \quad \mu_4 = 176.028, \quad \mu_5 = -72.761,\end{aligned}\right\} \tag{18}$$

which is displayed in figure 1.

On the free surface $\bar{y} = \bar{h}(\bar{x})$, with slope $\gamma = \bar{h}'(\bar{x})$,

$$\left.\begin{aligned}(1+\gamma^2)\bar{t}_n &= \gamma^2\bar{\sigma}_{xx}+\bar{\sigma}_{yy}-2\gamma\bar{\sigma}_{xy} = 0, &(19a)\\ (1+\gamma^2)\bar{t}_s &= \gamma(\bar{\sigma}_{yy}-\bar{\sigma}_{xx})+(1-\gamma^2)\bar{\sigma}_{xy} = 0 &(19b)\end{aligned}\right\} \quad (\bar{y} = \bar{h}),$$

and the accumulation condition is

$$\gamma\bar{u}-\bar{v} = \bar{q} \quad (\bar{y} = \bar{h}). \tag{20}$$

4. Leading-order balances

In contrast with the isothermal theory (Morland & Johnson 1980, 1982), the explicit dependence on variable $a(T)$ must be retained, but the same coordinate scaling and perturbation analysis again leads to a much simpler leading-order approximation (Morland 1983). The thermomechanically coupled equations are reduced to a convenient parabolic system, but here, with $T(x, y)$ prescribed, we again obtain a second-order ordinary differential equation for the profile $y = h(x)$.

In terms of the dimensionless variables (8) and (9), the deviatoric constitutive relations (2) and (3) become

$$\bar{\boldsymbol{S}} = \nu\frac{\phi(\hat{I})}{\bar{a}(\bar{T})}\bar{\boldsymbol{D}}, \tag{21}$$

$$J = s^{-2}(\bar{S}_{xx}^2+\bar{S}_{xy}^2), \quad \hat{I} = \frac{\delta^2}{\bar{a}^2}(\bar{D}_{xx}^2+\bar{D}_{yy}^2), \tag{22}$$

where

$$\nu = s\delta, \quad s = \frac{\sigma_0}{\rho g d_0}, \quad \delta = \frac{a_m}{d_0 D_0 a_0}. \tag{23}$$

With the units (6), a typical accumulation magnitude $q_m = 1$ m a^{-1}, and a minimum scale factor $a_0 = 0.2$,

$$\nu \approx 5 \times 10^{-3} \times \left(\frac{100 \text{ m}}{d_0}\right)^2 \approx 10^{-3} \to 5 \times 10^{-6} \quad \text{for} \quad d_0 = 200\text{–}3000 \text{ m}, \tag{24}$$

that is,

$$\nu \ll 1 \tag{25}$$

for a wide range of conditions. Unlike the isothermal case $\bar{a} \equiv 1$, we cannot assert that $\bar{\boldsymbol{S}} = O(\nu \bar{\boldsymbol{D}})$, since $\bar{a}(\bar{T})$ becomes increasingly smaller (table 1) as the temperature decreases. However, with $\bar{a} \approx 10^{-3}$ at an extreme $T = 233$ K, $\nu/\bar{a} \lesssim 10^{-2}$ for $d_0 \gtrsim 2000$ m, so a small parameter $\nu_m = \nu/\bar{a}_{\min}$ could be introduced. As d_0 decreases we expect $\bar{a}_{\min}$ to increase, that is, $T_{\min}$ to increase. However, since the equilibrium equations (12) and free-surface conditions (15) imply that $\bar{\sigma}_{yy}$ and $\bar{\sigma}_{xx}$ are order-unity quantities and that $\bar{\sigma}_{xy}$ must vary smoothly with $\bar{y}$ with maximum magnitude at the bed, it can be inferred that $\bar{\boldsymbol{D}}/\bar{a}$ varies smoothly. That is, $\bar{\boldsymbol{D}}$ decreases in magnitude as $\bar{a}$ decreases to maintain a smoothly varying and bounded ratio $\bar{D}/\bar{a}$, so we now interpret (21) as $\bar{\boldsymbol{S}} = O(\nu \bar{\boldsymbol{D}}/\bar{a})$, determine the scaling required by horizontal equilibrium as before, then obtain the associated strain-rate field $\bar{\boldsymbol{D}}$. The leading-order solution is found to be consistent with the perturbation scheme.

Following Morland & Johnson (1980, 1982), a series expansion in ν, which assumes that $\bar{\boldsymbol{D}}/\bar{a}$ remains of order unity everywhere, again yields an ice reservoir with horizontal free surface as the leading-order approximation, in which the vertical gradient of shear stress is negligible in comparison with the horizontal pressure gradient. As before, the shear-stress gradient is restored by a coordinate and stream-function scaling

$$\xi = \epsilon \bar{x}, \quad \Psi = \epsilon \bar{\psi} \quad (\epsilon \ll 1), \tag{26a,b}$$

such that ξ- and $\bar{y}$-derivatives have equal status, and

$$U = \epsilon \bar{u} = \frac{\partial \Psi}{\partial \bar{y}}, \quad \bar{v} = -\frac{\partial \Psi}{\partial \xi} \tag{27}$$

are order-unity quantities, the latter imposed by the original velocity scaling with unit q_m. Thus $\bar{u} = O(\epsilon^{-1})$, and setting

$$\bar{h}(\bar{x}) = H(\xi), \quad \Gamma = H'(\xi) = O(1), \quad \gamma = \epsilon \Gamma \tag{28}$$

shows that ϵ is the surface-slope magnitude. Now

$$\bar{\sigma}_{xy} = \frac{\nu}{\epsilon} \frac{\phi(\hat{I})}{\bar{a}(\bar{T})} \left\{ \frac{1}{2} \frac{\partial^2 \Psi}{\partial \bar{y}^2} - \tfrac{1}{2} \epsilon^2 \frac{\partial^2 \Psi}{\partial \xi^2} \right\}, \tag{29a}$$

$$\begin{pmatrix} \bar{\sigma}_{xx} \\ \bar{\sigma}_{yy} \end{pmatrix} = -\bar{p} \pm \nu \frac{\phi(\hat{I})}{\bar{a}(\bar{T})} \frac{\partial^2 \Psi}{\partial \xi \, \partial \bar{y}}, \tag{29b}$$

and the equilibrium equations (12) become

$$\epsilon \frac{\partial \bar{\sigma}_{xx}}{\partial \xi} + \frac{\partial \bar{\sigma}_{xy}}{\partial \bar{y}} = 0, \quad \epsilon \frac{\partial \bar{\sigma}_{xy}}{\partial \xi} + \frac{\partial \bar{\sigma}_{yy}}{\partial \bar{y}} = 1. \tag{30}$$

Hence the horizontal balance requires

$$\epsilon^2 = \nu, \tag{31}$$

and the vertical balance with free-surface condition (19a) then gives

$$\bar{\sigma}_{yy} = -[H(\xi)-\bar{y}]+O(\epsilon^2), \tag{32}$$

and in turn the horizontal balance with free-surface condition (19b) shows that

$$\bar{\sigma}_{xy} = -\epsilon\Gamma(\xi)\,[H(\xi)-\bar{y}]+O(\epsilon^3). \tag{33}$$

These results, which determine the leading-order $\bar{\sigma}_{yy} = \bar{\sigma}_{xx}$ and $\bar{\sigma}_{xy}$ in terms of $H(\xi)$ independent of the stream function Ψ, suppose that

$$\left\{\frac{\phi}{\bar{a}}\frac{\partial^2\Psi}{\partial\bar{y}^2}\right\}, \quad \left\{\frac{\phi}{\bar{a}}\frac{\partial^2\Psi}{\partial\xi\,\partial\bar{y}}\right\}, \tag{34a, b}$$

and their ξ-derivatives, remain of order unity throughout the sheet; which we find self-consistent with the stream function determined by the shear stress (33) and constitutive relative (29). In cold regions where $\bar{a}$ is small, $\partial^2\Psi/\partial\bar{y}^2$ and $\partial^2\Psi/\partial\xi\,\partial\bar{y}$ are necessarily small, and in warm regions where $\bar{a} \sim 1$ the strain rates are restricted by the bounded stress. It is the coordinate scaling (26a), defining a long-aspect-ratio sheet, which imposes the order of magnitude $\bar{\sigma}_{xy} = O(\epsilon)$ and hence the bound on $(\partial^2\Psi/\partial\bar{y}^2)/\bar{a}$ independent of ν, but the leading-order approximation (33) and resulting stream-function approximation require that the longitudinal deviatoric stress $\bar{\sigma}_{xx}-\bar{\sigma}_{yy}$ and its ξ-derivative are small; that is, $\nu \ll 1$ and conditions imposed on the expression (34b) apply. Since a thermal boundary layer associated with a warm basal region would enhance $\bar{y}$-derivatives at the expense of ξ-derivatives, and only ξ-derivative terms have been neglected in the $O(\epsilon^2)$ contributions above, the present leading-order equations are valid for a thermal boundary layer in which $\bar{T}$ varies rapidly with $\bar{y}$.

The leading-order invariants are given by

$$J = s^{-2}\{\bar{\sigma}_{xy}^2+O(\epsilon^4)\}, \quad \hat{I} = \frac{\theta}{\bar{a}^2}\left\{\left(\frac{1}{2}\frac{\partial^2\Psi}{\partial\bar{y}^2}\right)^2+O(\epsilon^2)\right\}, \tag{35}$$

where

$$\theta = \delta/s. \tag{36}$$

The remaining surface condition (20) becomes

$$\Gamma\frac{\partial\Psi}{\partial\bar{y}}+\frac{\partial\Psi}{\partial\xi} = \left.\frac{\mathrm{d}\Psi}{\mathrm{d}\xi}\right|_{\bar{y}=H} = \bar{q} \quad (\bar{y} = H(\xi)), \tag{37}$$

and the basal-drainage condition (13) becomes

$$\beta\frac{\partial\Psi}{\partial\bar{y}}+\frac{\partial\Psi}{\partial\xi} = \left.\frac{\mathrm{d}\Psi}{\mathrm{d}\xi}\right|_{\bar{y}=F} = \bar{b}, \quad \beta = F'(\xi) \quad (\bar{y} = f(\bar{x}) = F(\xi)), \tag{38}$$

where it is supposed that $|\beta| \lesssim 1$; that is, the bed slope does not exceed ϵ in magnitude. Finally, the basal tractions (15) and tangential velocity (14) are given by

$$\left.\begin{aligned} &\bar{t}_n = \bar{\sigma}_{yy}+O(\epsilon^2), \quad \bar{t}_s = \bar{\sigma}_{xy}+O(\epsilon^3), \\ &\bar{u}_s = \epsilon^{-1}\left\{-\frac{\partial\Psi}{\partial\bar{y}}+O(\epsilon^2)\right\} \end{aligned}\right\} \quad (\bar{y} = F(\xi)), \tag{39}$$

so that the sliding relation (16), with definitions (17), becomes

$$\bar{\sigma}_{xy} = -2.5\times10^{-5}\epsilon^{-1}\bar{\sigma}_{yy}\tilde{\mu}(-k\bar{\sigma}_{yy})\frac{\partial\Psi}{\partial\bar{y}}\{1+O(\epsilon^2)\} \quad (\bar{y} = F(\xi)). \tag{40}$$

It can be shown from the above system of equations that a series solution $H = H_0(\xi)+\epsilon^2 H_2(\xi)+\ldots$, $\Psi = \Psi_0+\epsilon^2\Psi_2+\ldots$, in ϵ^2 is appropriate; that is, the correction to the leading-order solution is of order $\epsilon^2 = \nu$, not order ϵ (Morland 1983).

5. Solution for prescribed temperature

Given $\bar{T}(\bar{x},\bar{y})$, then $\bar{a}(\bar{T})$ is a known function $\hat{a}(\xi,\bar{y})$. Let $H(\xi)$, $\Gamma(\xi)$, $\Psi(\xi,\bar{y})$ and $p(\xi,\bar{y})$ denote the respective leading-order approximations (omitting a subscript 0), all of order unity, then the leading-order shear stresses are

$$\left.\begin{aligned}\bar{\sigma}_{xy} &= -\epsilon\Gamma(\xi)\,[H(\xi)-\bar{y}] = \epsilon\frac{\phi}{\hat{a}}\left(\frac{1}{2}\frac{\partial^2\Psi}{\partial\bar{y}^2}\right) = O(\epsilon),\\ \bar{\sigma}_{xx}-\bar{\sigma}_{yy} &= 2\epsilon^2\frac{\phi}{\hat{a}}\frac{\partial^2\Psi}{\partial\xi\,\partial\bar{y}} = O(\epsilon^2).\end{aligned}\right\} \tag{41}$$

Hence, to leading order, using the relations (35), (36), (29a), and (31),

$$J = s^{-2}\bar{\sigma}_{xy}^2 = \hat{I}\phi^2(\hat{I}), \tag{42}$$

and the reciprocal relations (5) yield

$$\hat{I} = s^{-2}\bar{\sigma}_{xy}^2\,\omega^2(s^{-2}\bar{\sigma}_{xy}^2). \tag{43}$$

Thus, from the relations (35) and (41),

$$\frac{\partial^2\Psi}{\partial\bar{y}^2} = \zeta\hat{a}(\xi,\bar{y})\,g[-\zeta\Gamma(H-\bar{y})], \quad \zeta = -\operatorname{sgn}(\Gamma), \tag{44}$$

where ζ is introduced to select the appropriate square root of $\hat{I}$ as Γ changes sign, and

$$g(t) = 2t\omega(\theta t^2) \quad (t \geqslant 0). \tag{45}$$

For the constitutive model (7), $g(t)$ is a polynomial with terms in t, t^3 and t^5.

Define

$$\left.\begin{aligned}\hat{g}_1(\xi,\bar{y}) &= \int_{F(\xi)}^{\bar{y}}\hat{a}(\xi,\bar{y}')\,g[-\zeta\Gamma(H-\bar{y}')]\,\mathrm{d}\bar{y}',\\ \hat{g}_2(\xi,\bar{y}) &= \int_{F(\xi)}^{\bar{y}}\hat{g}_1(\xi,\bar{y}')\,\mathrm{d}\bar{y}',\end{aligned}\right\} \tag{46}$$

both vanishing on the bed $\bar{y} = F(\xi)$. In the isothermal case $\hat{a} \equiv 1$, analogous functions g_1 and g_2 were introduced which vanished on the surface $\bar{y} = H(\xi)$ (Morland & Johnson 1982). Integration from the given bed is more convenient here. Integrating the second derivative (44) gives

$$\epsilon\bar{u} = \frac{\partial\Psi}{\partial y} = -\epsilon\bar{u}_s(\xi)+\zeta\hat{g}_1(\xi,\bar{y}), \tag{47}$$

where $\bar{u}_s$ is the leading-order tangential velocity defined by (39) and satisfying a sliding law (40). Integrating again,

$$\Psi = \Psi_b(\xi)-\epsilon[\bar{y}-F(\xi)]\,\bar{u}_s(\xi)+\zeta\hat{g}_2(\xi,\bar{y}), \tag{48}$$

and by the basal-drainage condition (38),

$$\Psi_b'(\xi) = \bar{b}. \tag{49}$$

The accumulation condition (37) now gives

$$\frac{\mathrm{d}}{\mathrm{d}\xi}\{-\epsilon[H(\xi)-F(\xi)]\,\bar{u}_s(\xi)+\zeta\hat{g}_2[\xi,H(\xi)]\} = \bar{q}-\bar{b}. \tag{50}$$

In the isothermal case, when $\hat{a} \equiv 1$,

$$\hat{g}_2[\xi, H(\xi)] = [\zeta\Gamma(\xi)]^{-2} \int_0^{t_b} t' g(t')\, \mathrm{d}t', \quad t_b = -\zeta\Gamma(H-F), \tag{51}$$

which reduces the differential equation (50) to that derived by Morland & Johnson (1982).

When $\bar{u}_s(\xi)$ is expressed in terms of $H(\xi)$ and $\Gamma(\xi)$ by the sliding law (40) and stress expressions (32) and (33), (50) is a second-order differential equation for $H(\xi)$. There are two end conditions, $H = F$ at both margins, but their relative locations – the span – must be determined by the solution which has the additional integral property of zero net flux into the sheet from the steady-state assumption. However, like the isothermal case, the slope at either margin can be determined directly from the behaviour of the differential equation as $H \to F$. Let Γ_m, β_m denote the surface and bed slopes at a margin, $q_m^* = \bar{q} - \bar{b}$ and $\bar{u}_m = \bar{u}_s$ at the same margin. By the definitions (46), $\mathrm{d}g_2[\xi, H(\xi)]/\mathrm{d}\xi \to 0$ as $H \to F$, so letting $H \to F$ in the differential equation (50) gives the result

$$\epsilon \bar{u}_m(\Gamma_m - \beta_m) = -q_m^*, \tag{52}$$

which is independent of $\bar{a}(\bar{T})$. Applying the sliding law (40) in the limit $H \to F$ shows that

$$\epsilon \bar{u}_m = 4 \times 10^4 \frac{\epsilon^2 \Gamma_m}{\tilde{\mu}(0)}, \tag{53}$$

and hence

$$\Gamma_m(\Gamma_m - \beta_m) = -2.5 \times 10^{-5} \epsilon^{-2} \tilde{\mu}(0)\, q_m^* > 0, \tag{54}$$

since at a right margin

$$\bar{u} > 0 \Rightarrow \bar{u}_s < 0, \quad \bar{\sigma}_{xy} > 0, \quad \Gamma_m < 0, \quad \zeta = +1, \quad \text{and necessarily} \quad \Gamma_m - \beta_m < 0,$$

and at a left margin

$$\bar{u} < 0 \Rightarrow \bar{u}_s > 0, \quad \bar{\sigma}_{xy} < 0, \quad \Gamma_m > 0, \quad \text{and necessarily} \quad \Gamma_m - \beta_m > 0.$$

Thus

$$q_m^* < 0, \tag{55}$$

is a necessary condition; that is, net outflow at a margin. The quadratic (54) has unique positive and negative roots Γ_m defining the left and right margin slopes. The second-order differential equation (50) can be integrated from either margin with prescribed $H = F$ and $H' = \Gamma_m$, and the far margin is located when $H - F \to 0$. This is a standard numerical problem, but a bed topography $F(\xi)$, in contrast with a flat bed $F \equiv 0$, leads in general to a narrow region of large slope before a far margin is reached (Morland & Johnson 1982). A finite-slope 'boundary layer' may extend the solution to a far margin. Alternatively, Dr K. Hutter suggests (private communication) that a small adjustment of the starting margin with respect to the topography may yield a small-slope steady-state solution valid up to a far margin.

As in the isothermal case, (50) can be used as an algebraic equation to determine $\bar{u}_s(\xi)$, and in turn the function $\mu(-\dot{\epsilon}_n)$ in a sliding law of the form (16), if the profile $H(\xi)$ is prescribed in addition to $\bar{q}$, $\bar{b}$ and $\bar{T}$. With the profile and accumulation data used by Morland *et al.* (1983) for a Greenland Ice Sheet section, together with a temperature distribution constructed by L. D. Williams (private communication), we have determined the corresponding sliding function $\tilde{\mu}(\tilde{p}_b)$ defined by the relations (16) and (17), which is displayed in figure 1. This modified sliding law is also used to express equation (50) as a differential equation for $H(\xi)$, and to investigate the influence of the different temperature patterns.

Recall that validity of the above leading-order expressions required that ξ-derivatives of the stream function do not exceed order unity. We can now see that ξ-derivatives will remain of order unity if appropriate derivatives of $F(\xi)$ remain of order unity provided that the sliding law is smooth; that is, there is no abrupt change of sliding resistance. Clearly, abrupt changes of sliding resistance or bed topography must enhance the local status of ξ-derivatives, which bring into play the longitudinal deviatoric stress and annuls the simple leading-order expression (33) for the direct shear stress.

6. Accumulation and temperature patterns

Our main purpose is to demonstrate the effects of temperature distribution, so we focus on a simple accumulation/ablation pattern, that labelled 4($\frac{1}{2}$) in the Boulton *et al.* (1983) application of the isothermal theory. In this, $\bar{q}$ depends only on elevation, having linear dependence below the equilibrium-line altitude h_e, cubic dependence between h_e and $h_s = h_e + 500$ m, and is constant above h_s, with $\bar{q}$ and $\mathrm{d}\bar{q}/\mathrm{d}h$ continuous at h_e and h_s. For the comparison of profiles predicted by different temperature patterns we introduce common normalized coordinates by taking

$$d_0 = 2000 \text{ m}, \quad \epsilon_0 = 0.005, \quad \bar{\xi} = \epsilon_0 \bar{x} = \epsilon_0 s^{-1} \delta^{-1} \xi, \tag{56}$$

for all cases, so that the $\bar{y}$- and H-unit is 2000 m and the $\bar{\xi}$-unit is 400 km. The associated longitudinal velocity unit is $q_m/\epsilon_0 = 200$ m a^{-1}. The accumulation pattern is

$$\bar{q} = \left\{ \begin{array}{ll} 12.5\,(H - H_e) & (H \leqslant H_e), \\ 12.5\,(H - H_e) - 76(H - H_e)^2 + 136(H - H_e)^3 & (H_e \leqslant H \leqslant H_e + 0.25), \\ 0.5 & (H \geqslant H_e + 0.25). \end{array} \right\} \tag{57}$$

We adopt $h_e = 1000$ m ($H_e = 0.5$) for the main series of computations, but investigate a sequence of h_e between 1000 and 1500 m for one temperature pattern to investigate the influence of equilibrium line altitude.

The prescription of temperature and temperature gradient along the surface and base required by the features (i)–(iii) described in §1 can be most simply incorporated in a temperature representation that is cubic in $\bar{y}$ with coefficients depending on $\bar{\xi}$. Thus

$$T(\bar{\xi}, \bar{y}) = c_0(\bar{\xi}) + c_1(\bar{\xi})\,\bar{y} + c_2(\bar{\xi})\,\bar{y}^2 + c_3(\bar{\xi})\,\bar{y}^3, \tag{58}$$

where

$$\left. \begin{array}{l} c_0 = T_b - \dfrac{\partial T_b}{\partial \bar{y}} \bar{F} + r_1 \bar{F}^2 - r_2 \bar{F}^3, \quad c_3 = r_2, \\ c_1 = \dfrac{\partial T_b}{\partial \bar{y}} - 2 r_1 \bar{F} + 3 r_2 \bar{F}^2, \quad c_2 = r_1 - 3 r_2 \bar{F}, \end{array} \right\} \tag{59}$$

and

$$\left. \begin{array}{l} r_1 = (\bar{H} - \bar{F})^{-2} \left\{ 3(T_s - T_b) - (\bar{H} - \bar{F}) \left(2 \dfrac{\partial T_b}{\partial \bar{y}} + \dfrac{\partial T_s}{\partial \bar{y}} \right) \right\}, \\ r_2 = (\bar{H} - \bar{F})^{-3} \left\{ 2(T_b - T_s) + (\bar{H} - \bar{F}) \left(\dfrac{\partial T_b}{\partial \bar{y}} + \dfrac{\partial T_s}{\partial \bar{y}} \right) \right\}. \end{array} \right\} \tag{60}$$

Here T_b denotes T and $\partial T_b/\partial \bar{y}$ denotes $\partial T/\partial \bar{y}$ evaluated on the bed $\bar{y} = \bar{F}(\bar{\xi})$, and similarly T_s and $\partial T_s/\partial \bar{y}$ imply evaluation on the surface $\bar{y} = \bar{H}(\bar{\xi})$. Property (i) gives

$$T_s = T_m - 16 K \bar{H}(\bar{\xi}), \quad \frac{\partial T_s}{\partial \bar{y}} = 0, \tag{61}$$

where T_m is the margin temperature by choice of the margin as coordinate origin, and property (ii) gives

$$\frac{\partial T_b}{\partial \bar{y}} = -20 \text{ K} \quad \text{or} \quad -50 \text{ K}. \tag{62}$$

Since $\bar{H}(\bar{\xi})$ appears in the surface temperature T_s, the temperature field is calculated simultaneously with the profile as the differential equation is integrated in steps from the margin.

Finally, the different basal temperature properties (iii) are modelled by

$$T_b \equiv T_m, \quad T_b = T_m - T_1 \bar{\xi}, \tag{63a,b}$$

$$T_b = T_m + T_1 \bar{\xi}, \quad T_b = (273.15 - 6 + 18\bar{\xi} - 20\bar{\xi}^2)\,\text{K}, \tag{63c,d}$$

where T_1 is a positive temperature. In distribution (63d), the bed temperature increases from -6 °C at the margin to -1.95 °C at $\bar{\xi} = 0.45$ ($x = 180$ km), and then decreases. Uniform bed temperatures $T_m = -2, -6$ and -10 °C have been investigated for (63a), and in (63c) $T_m = -6$ °C, $T_1 = 4$ K, which represents a 4 K rise per 400 km. Various T_m and T_1 to describe monotonic cooling away from the margin in (63b) have also been investigated.

7. Profiles and flows

We now present surface profiles determined by the differential equation (50), and the associated longitudinal velocities given by expression (47), for the surface accumulation pattern (57) with zero basal drainage and the various temperature patterns described in §6, with $\partial T_b/\partial \bar{y} = -20$ K, and with the basal sliding velocity given by the relations (16)–(18). A flat bed is assumed so that basal effects due to temperature variation are not clouded by topography effects. With the equilibrium line altitude h_e fixed at 1000 m ($H_e = 0.5$), the margin slope determined by the relation (54) and margin velocity determined by the expression (52) are fixed, since the margin accumulation given by the relation (57) at $H = 0$ depends only on H_e. The scale factor a_0 in the rate factor (8) is assumed unity.

First, for comparison, we present some features of the isothermal solutions at $T = -23$ °C, $T = -15$ °C, $T = -2$ °C. Figure 2 shows the profile, basal sliding velocity, and longitudinal velocities relative to the bed at three vertical sections for $T = -23$ °C. For this relatively uniformly cold sheet, the differential motion between bed and surface accounts for only 10 % of the surface velocity, but nevertheless, as demonstrated by Morland & Johnson (1980), the contribution of the shear term in the differential equation (50) is significant. This proportion increases as the uniform temperature increases, and table 2 gives details for the three temperatures, with x denoting distance from the margin, x_d distance to the divide where the surface slope vanishes (or semispan, since the flat-bed profile is symmetric about the divide), and h_d is the thickness at the divide. As T is increased, the rate of shear strain increases at a given stress, particularly as the melting point is approached, which is reflected by the increased proportion of differential motion. The shear-stress distribution, which depends on the surface height and surface slope, does not change dramatically between the three temperatures. The moderate span increase and thickness decrease correspond to a moderate slope decrease (at each point) as T is increased, which implies a decrease of basal shear stress and velocity (except at the divide and the margin), and hence an increased differential motion to balance the fixed accumulation.

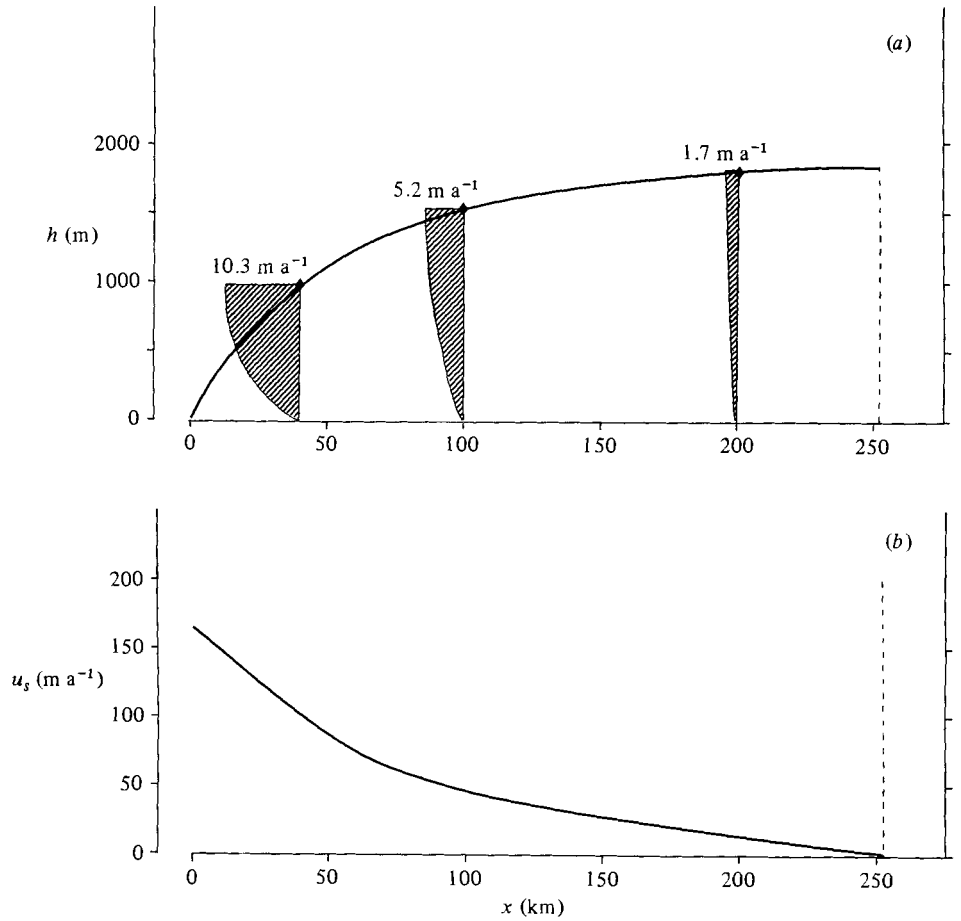

FIGURE 2. Isothermal solution at $T = -23$ °C: (*a*) surface profile and longitudinal velocities relative to the basal velocity; (*b*) basal-velocity distribution.

T \ x	40 km		100 km		200 km		x_d	h_d
−23 °C	$u_H = 110$ $u_F = 100$	(9.1 %)	52 46	(11.5 %)	15 13	(13.3 %)	252 km	1856 m
−15 °C	$u_H = 121$ $u_F = 94$	(22.3 %)	59 44	(25.4 %)	18 13	(27.8 %)	259 km	1802 m
−2 °C	$u_H = 197$ $u_F = 66$	(66.5 %)	132 32	(75.8 %)	60 13	(78.3 %)	329 km	1564 m

TABLE 2. Surface and basal longitudinal velocities u_H, u_F, in m a^{-1}, at three distances x from margin; x_d is the semi-span, h_d is the maximum thickness

Next consider uniform bed temperatures $T_b = -2$ °C and $T_b = -6$ °C in the prescribed temperature pattern. The temperature variation with height at three sections, together with the resulting profile, basal velocity and relative longitudinal velocity at three sections, are shown in figures 3 and 4. For the moderately warmer bed (figure 3) the temperature influence on the rate factor is reflected by the increased differential motion, but there is negligible change of span and only a modest decrease

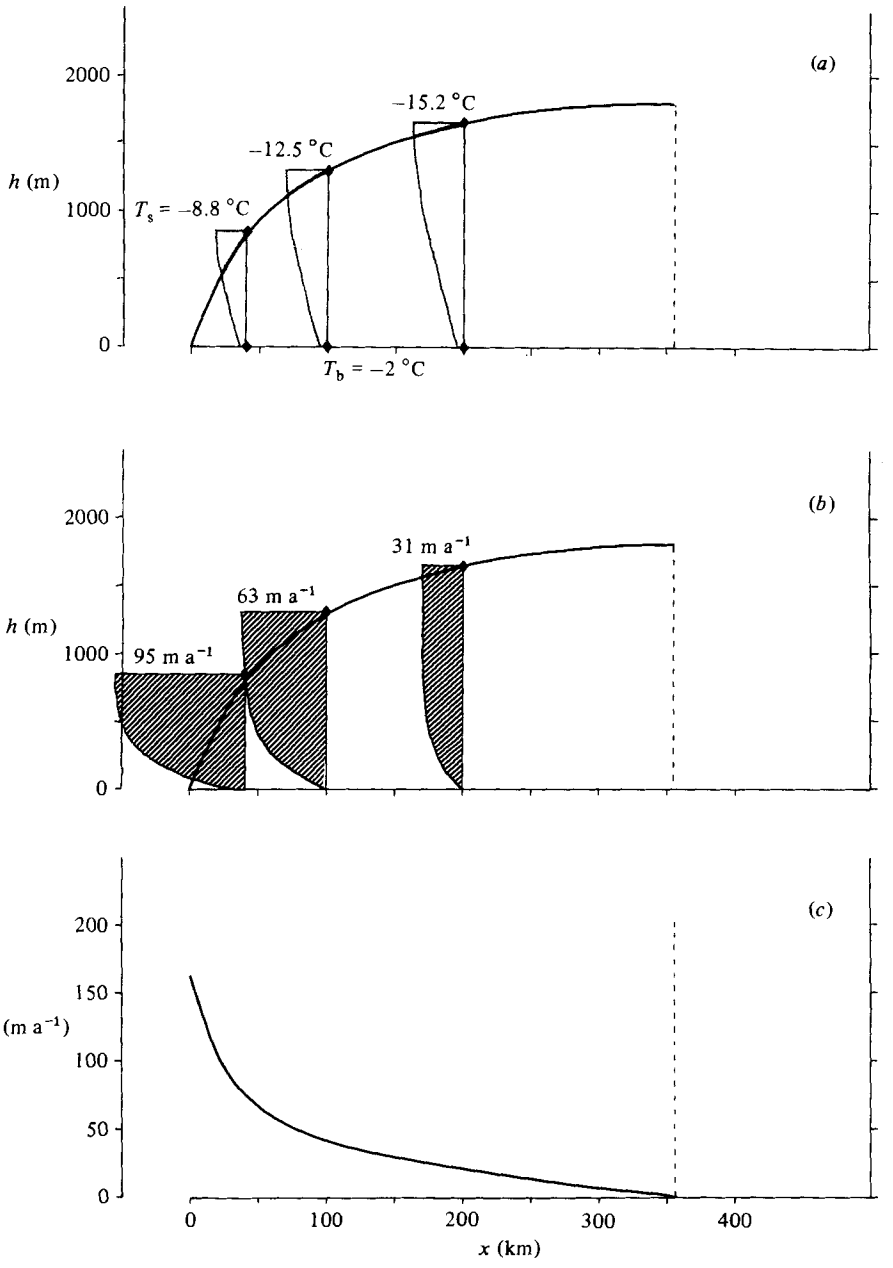

FIGURE 3. Solution for temperature variation with uniform bed temperature $T_b = -2$ °C: (*a*) profile and temperature variation; (*b*) longitudinal velocities relative to the basal velocity; (*c*) basal-velocity distribution.

in maximum thickness in comparison with figure 4. The span is moderately larger than the warm isothermal solution ($T = -2$ °C), but much greater than the colder isothermal solution, while the maximum thickness is closer to the colder isothermal solutions. It is evident that there is no optimum mean-temperature solution which approximates to the temperature-dependent solutions for these simple temperature patterns, and that the change of velocity distribution accompanying the temperature

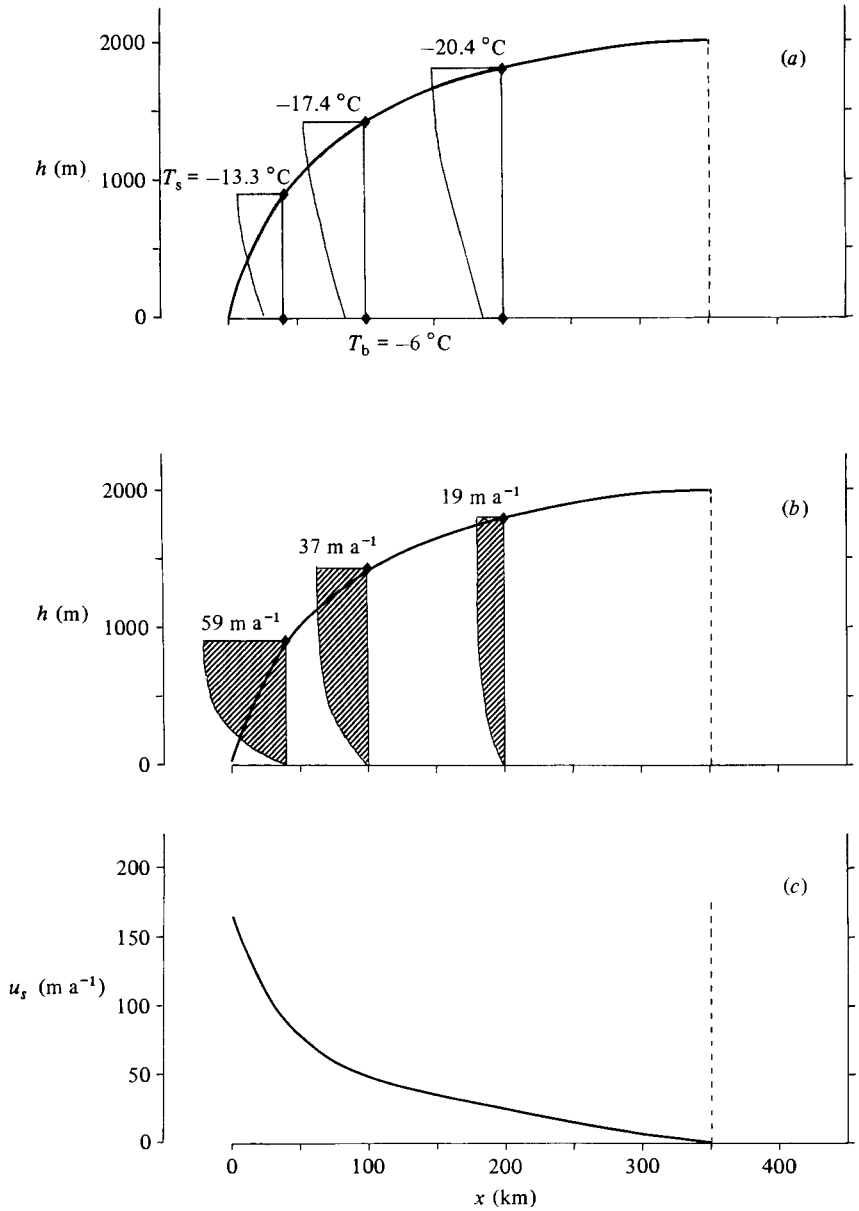

FIGURE 4. Solution for temperature variation with uniform bed temperature $T_b = -6$ °C: (*a*) profile and temperature variation; (*b*) longitudinal velocities relative to the basal velocity; (*c*) basal-velocity distribution.

variation influences the large-scale features significantly. Moreover, the enhanced velocity gradients extend well beyond a negligible boundary layer, and reinforce the earlier isothermal-analysis conclusion (Morland & Johnson 1980) that the shear term contributes significantly to the profile equation.

When solutions for monotonic decrease of the bed temperature away from the margin, (63*b*), are attempted, with non-trivial rate of decrease, a divide is not reached. A qualitative explanation is that the shear motion becomes negligible as

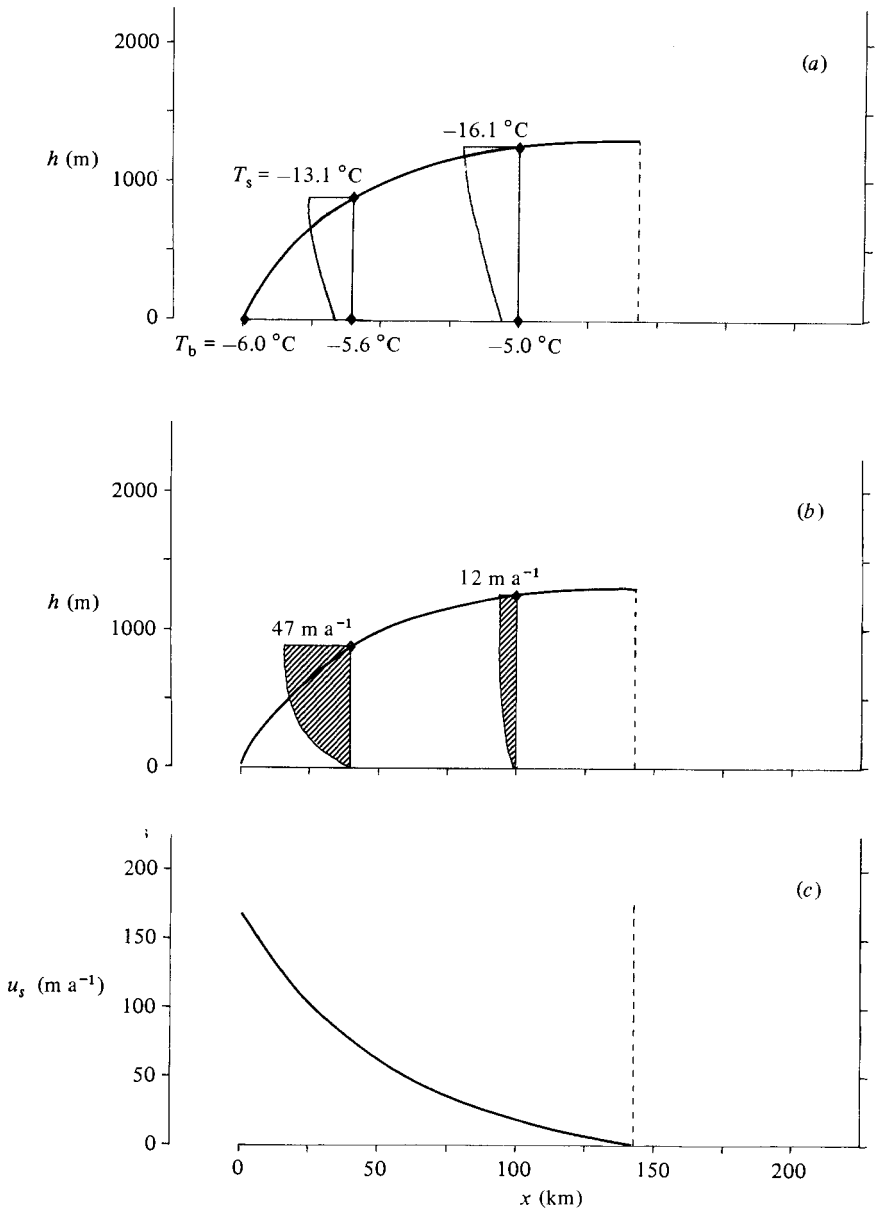

FIGURE 5. Solution for temperature variation with bed temperature linearly increasing with distance from margin; $T_b = -6\ °C + (4\ °C)\,\xi$: (*a*) profile and temperature variation; (*b*) longitudinal velocities relative to the basal velocity; (*c*) basal-velocity distribution.

the temperature decreases, both with distance from the margin and with height above the bed, so that a given accumulation must be carried by basal sliding, which implies non-zero basal shear stress and non-zero surface slope.

Now consider (63*c*) with the bed temperature increasing monotonically away from the margin at a rate 1 K per 100 km and a margin temperature −6 °C. The results are shown in figure 5. By comparison with a uniform bed temperature −6 °C (figure 4), there are dramatic decreases of span and maximum thickness, and significant

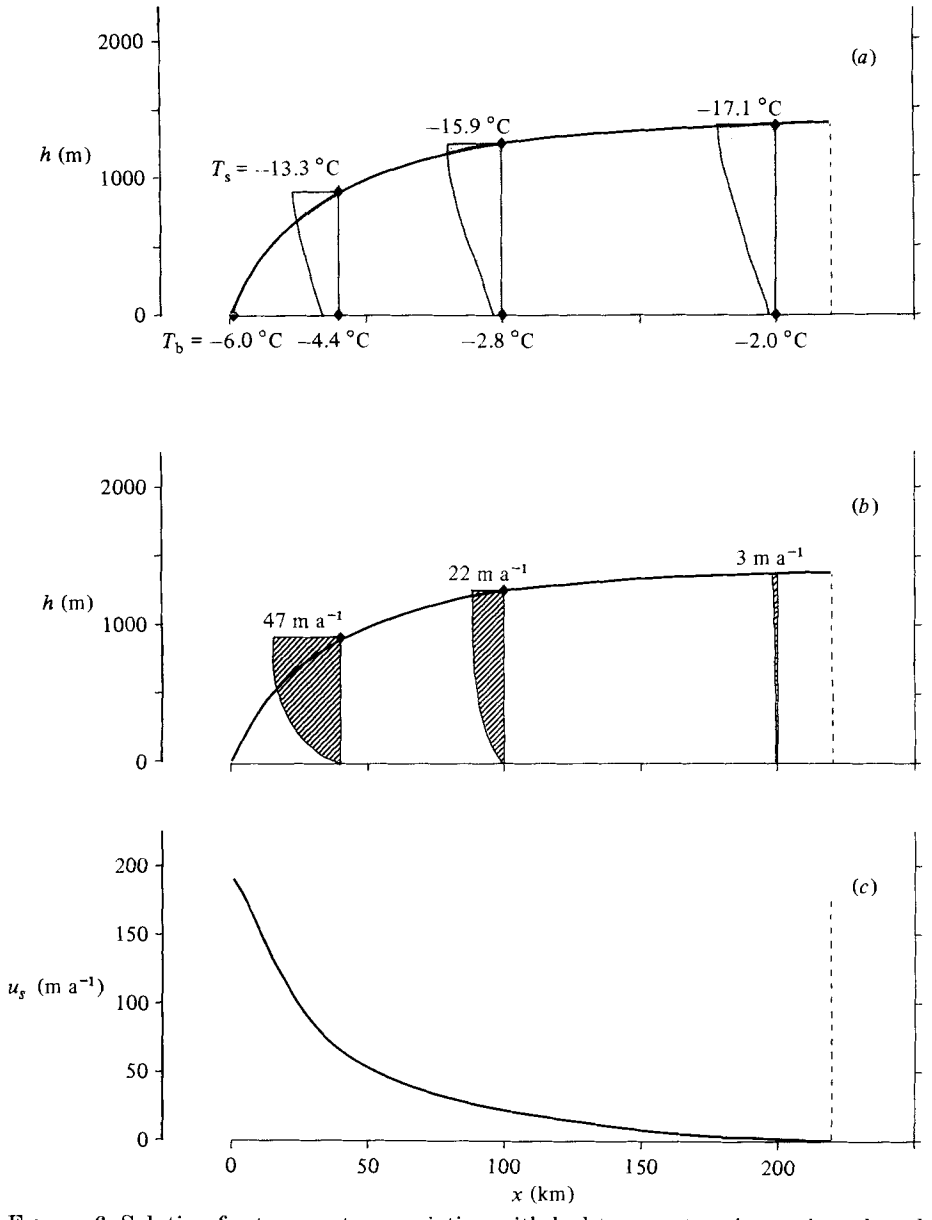

FIGURE 6. Solution for temperature variation with bed temperature increasing, then decreasing, with distance from margin; $T_b = -6\ °C + (18\ °C)\,\xi - (20\ °C)\,\xi^2$: (*a*) profile and temperature variation; (*b*) longitudinal velocities relative to the basal velocity; (*c*) basal-velocity distribution.

decreases in the differential motion between bed and surface, even though the longitudinal warming is so small, again reflecting the strong temperature dependence of the rate factor near melting. Recall that an increase of temperature in the isothermal solution causes an increase of span (table 2), emphasizing that temperature distribution, longitudinally as well as vertically, has a significant role.

Finally, the quadratic distribution (63*d*) describes increasing then decreasing bed temperature away from the margin, with margin temperature −6 °C and maximum

temperature -1.95 °C at distance 180 km. Here the equilibrium line altitude (ELA) h_e in the accumulation pattern (57) was varied between 1000 and 1500 m. At ELAs 1300 and 1400 m a finite semispan x_d exceeding 180 km was obtained, so a decreasing-bed-temperature zone was included, but at ELA 1500 m a divide was not reached, similar to (63*b*). The results are shown in figure 6 for the ELA of 1300 m, but comparison with the monotonic warming results of figure 5 is not useful since they correspond to an ELA of 1000 m. Here we have demonstrated that a basal-temperature cooling towards the divide is acceptable provided that there has been sufficient flux in the accumulation zone to balance the ablation. It may be that a basal-temperature cooling away from the margin will provide a finite span for different accumulation patterns or basal sliding.

For the larger basal temperature gradient $\partial T_b/T\bar{y} = -50$ K and the uniform basal temperatures $T_b = -2$ and -6 °C, the small-surface-slope solution fails before a divide is reached. Here the more dramatic cooling away from the base appears to eliminate the internal deformation required to balance the surface accumulation. This is similar to the explanation offered for the failure of (63*b*) with the smaller vertical temperature gradient. However, when basal temperature patterns (63*c*, *d*) with warming away from the margin are adopted, solutions with finite spans are obtained again, but both span and thickness are significantly greater. This reflects the smaller rate of internal deformation associated with colder ice. It is evident that the interplay of temperature pattern and internal flow is important, and physically compatible temperature and velocity fields are only guaranteed by solution of the thermomechanically coupled flow equation.

8. Modified sliding law

For given profile, temperature distribution and accumulation distribution, (50) becomes an algebraic equation for the basal sliding velocity $\bar{u}_s(\xi)$, and the basal pressure and shear traction are given by (32) and (33). Adopting the profile and steady accumulation data for the 70° N section of West Greenland used by Morland *et al.* (1983) in the corresponding isothermal theory, together with a temperature distribution constructed by L. D. Williams (private communication) from an approximate thermal analysis proposed by Jones (1978), we have determined the implied function $\tilde{\mu}(\tilde{p}_b)$ when a linear sliding law of the separable form (16) is assumed. The profile and temperature contours are shown in figure 7 (*a*), which also indicate a zone of basal melting. With the scale factor $a_0 = 1$, the predicted basal velocity is directed away from the margin over a large part of the bed, curve ① in figure 7 (*b*), and a reduced scale factor, to decrease the differential motion and thus increase the basal velocity (towards the margin) is required to achieve a physically sensible result. Curves ② and ③ correspond to $a_0 = \frac{1}{2}$ and $a_0 = \frac{1}{3}$ respectively, and the latter gives a correct direction of sliding everywhere. Figure 7 (*c*) shows longitudinal velocity distributions for $a_0 = \frac{1}{3}$ when the bed topography is incorporated.

However, the basal velocity is still non-monotonic, and incompatible with a single-valued sliding relation. A smoother distribution is obtained by neglecting the bed topography; that is, assuming a mean flat bed, and is shown as curve ④, but the non-monotonic feature remains. Thus the non-monotonic velocity is not a consequence of the bed topography, but results from the local non-monotonic surface slope in the adopted profile. That is, while the surface profile is not sensitive to moderate variation of a prescribed sliding function $\tilde{\mu}(\tilde{p}_b)$, the sliding velocity and associated function $\tilde{\mu}(\tilde{p}_b)$ required for a given profile are strongly sensitive to local

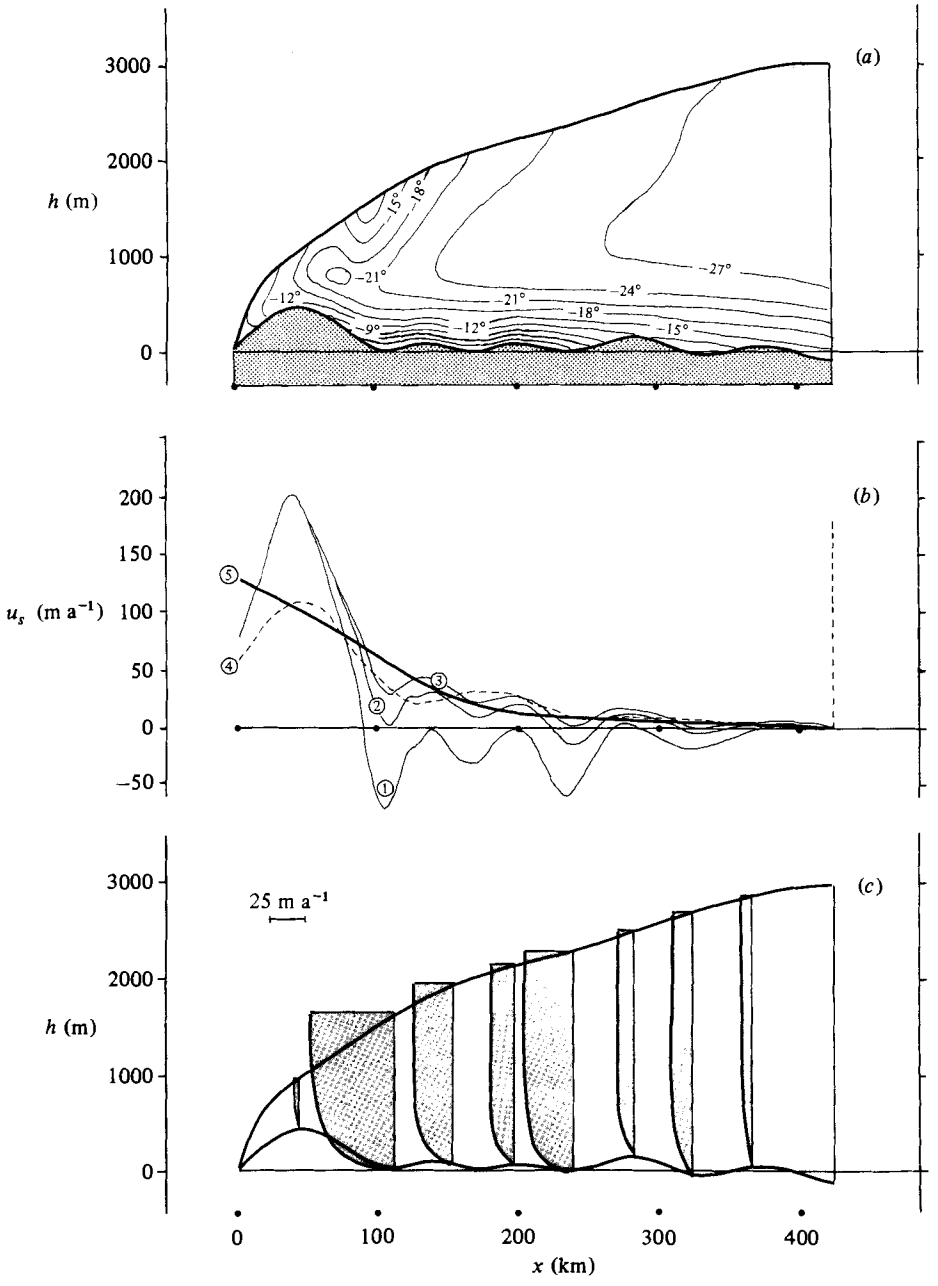

FIGURE 7. (*a*) Profile and temperature contours for the 70° N section of West Greenland. (*b*) Basal-velocity distributions: ①, $a_0 = 1$; ②, $\frac{1}{2}$; ③, $\frac{1}{3}$; ④, $\frac{1}{3}$, flat bed at sea level; ⑤, $\frac{1}{3}$, flat bed at sea level, smoothed surface contour. (*c*) Longitudinal velocities relative to the basal velocity for case ③ above.

changes in the surface slope and associated basal shear stress. It is therefore not sensible to incorporate small-scale variations of surface slope inferred from observation. Smoothing of the profile leads to a physically acceptable distribution (curve ⑤), and in turn to the function $\tilde{\mu}(\tilde{p}_b)$ shown in figure 1 for comparison with the isothermally deduced law.

Repeating the profile constructions for the various temperature patterns with the modified sliding law gives little difference in the overall solutions. The chief reason is that the two sliding functions $\tilde{\mu}(\tilde{p}_b)$ (figure 1) are very similar for small $\tilde{p}_b$; that is, near the margin. It was concluded in the Boulton *et al.* (1983) isothermal study that it is a change of the sliding function $\tilde{\mu}(\tilde{p}_b)$ near the margin which produces significant changes of span and maximum thickness, and that profiles are much less sensitive to changes of sliding function in the central zone with appreciable overburden. We suggest that the much simpler (and less controversial) non-slip condition could be adopted away from the margin for non-temperate basal conditions, with appropriate sliding as the overburden approaches zero so that the differential equation (50) is valid up to the margin, which is the starting point for the integration.

9. Concluding remarks

A plane steady-flow analysis has been used to demonstrate the significant effects of temperature distribution through an ice sheet caused by the strongly temperature-dependent viscous rate factor. While the temperature patterns are prescribed, without solution of the energy balance, we suggest that they are compatible with the limited observations available and cover a wide range of plausible variations. In order to focus on the influence of temperature, results for one surface accumulation distribution and one sliding law on a flat bed are presented, with comment on results for an alternative sliding law. Isothermal results (Boulton *et al.* 1983) have demonstrated that moderate variation of the accumulation distribution and of the basal sliding away from the margin do not have significant effects on the internal flow pattern.

We find that there is no optimum mean temperature for which the isothermal solution approximates satisfactorily to solutions for even simple temperature patterns varying only with depth. But also the enhanced velocity gradients in the warmer basal regions (of the temperature patterns considered) do not induce a high-shear-rate boundary layer with negligible shear rate through the bulk flow, which are the essential features of Nye's elementary model. That is, the viscous response of the ice is not confined, in general, to a thin basal boundary layer which can be replaced by a sliding discontinuity. This conclusion can also be inferred from a general analysis of the full thermomechanical balances (Morland 1983), but is based, of course, on the assumption of homogeneous ice properties throughout the sheet. If the older ice in the basal layer is significantly less viscous than the bulk of the ice sheet, then indeed the shear rate in the basal region would be further enhanced. It is also shown that very small variation of bed temperature with distance from the margin can have a significant effect on the internal flow and profile, so that both depth and longitudinal variation of temperature are important.

The sensitivity of the flow and profile solution to changes in an assumed temperature distribution suggests that flow predictions based on an extrapolation of a few measured temperature profiles with depth must be open to question. A solution of the thermomechanically coupled flow system, in which both vertical and horizontal advection, and internal dissipation, are significant, is essential to determine compatible flow and temperature fields. The iteration procedure (Hutter 1982, 1983) may exhibit unsatisfactory convergence properties because of the sensitivity to temperature change. Direct solution of the reduced parabolic system (Morland 1983) provides an alternative method which determines flow and temperature simultaneously, but a satisfactory numerical algorithm has not yet been constructed.

This work was supported by a NERC Grant GR3/4114: 'Relationship between glaciers and climate during the last glacial period in Northwest Europe'.

REFERENCES

BOULTON, G. S., SMITH, G. D. & MORLAND, L. W. 1983 The reconstruction of former ice sheets and their mass balance characteristics using a nonlinearly viscous flow model. *J. Glaciol.* (in the press).

GLEN, J. W. 1955 The creep of polycrystalline ice. *Proc. R. Soc. Lond.* A **228**, 515–538.

JOHNSON, R. E. & MCMEEKING, R. M. 1982 Near-surface flow in glaciers obeying Glen's Law. *Univ. Illinois T & AM Rep.* 454.

JONES, A. S. 1978 The dependence of temperature profiles in ice sheets on longitudinal variations in velocity and surface temperature. *J. Glaciol.* **20**, 31–39.

HUTTER, K. 1982 Dynamics of glaciers and large ice masses. *Ann. Rev. Fluid Mech.* **14**, 87–130.

HUTTER, K. 1983 *Theoretical Glaciology*, Reidel.

MELLOR, M. & TESTA, R. 1969 Effect of temperature on the creep of ice. *J. Glaciol.* **8**, 131–145.

MORLAND, L. W. 1983 Thermomechanical balances of ice sheet flows. Submitted to *Geophys. Astrophys. Fluid Dyn.*

MORLAND, L. W. & JOHNSON, I. R. 1980 Steady motion of ice sheets. *J. Glaciol.* **25**, 229–246.

MORLAND, L. W. & JOHNSON, I. R. 1982 Effects of bed inclination and topography on steady isothermal ice sheets. *J. Glaciol.* **28**, 71–90.

MORLAND, L. W. & SHOEMAKER, E. M. 1982 Ice shelf balances. *Cold Regions Sci. Tech.* **5**, 235–251.

MORLAND, L. W., SMITH, G. D. & BOULTON, G. S. 1983 Basal sliding relations deduced from ice sheet data. *J. Glaciol.* (in the press).

NYE, J. F. 1959 The motion of ice sheets and glaciers. *J. Glaciol.* **3**, 493–507.

SMITH, G. D. & MORLAND, L. W. 1981 Viscous relations for the steady creep of polycrystalline ice. *Cold Regions Sci. Tech.* **5**, 141–150.